Response to Reviews for the manuscript #egusphere-2025-156

We sincerely thank Referee #2 and the editor for reviewing and evaluating our manuscript entitled "Extreme carbon fluxes may result from autochthonous particulate organic carbon regulated by the interactions between picophytoplankton and heterotrophic bacteria in river-reservoir systems" (ID: egusphere-2025-156), and for providing us with valuable and constructive comments. These comments help us to improve the quality of the manuscript. We have revised the manuscript according to Referee #2's comments and provided detailed point-by-point responses to the comments. In the following, Referee #2's comments are shown in blue, and our responses are presented in black. The corresponding revisions have been highlighted in yellow in the revised manuscript.

Referee #2's key and minor comments and our responses are as follows:

Key comments included 15 points, which can be categorized into four aspects: (1) clarifying methodological details, (2) strengthening data interpretation, (3) refining statistical and ecological context, and (4) improving visualization and readability.

1) Aspect1 (extreme value classification): Provide goodness-of-fit metrics (e.g., Kolmogorov-Smirnov test) for the Pearson Type III distribution to validate its suitability for the dataset.

We thank you for pointing this out. We have used the Kolmogorov-Smirnov test to assess the differences between the measured data (i.e., CH_4 and CO_2 concentrations and fluxes of all samples) and theoretical distribution of Pearson type III frequency curve. The p-value from the Kolmogorov-Smirnov test has been added to Fig. S2, and

the descriptions regarding the use of the Kolmogorov-Smirnov test and fitness of the Pearson type III distribution have been included in section 2.5 of the revised manuscript and Supplementary Text S3 of the revised Supplementary Information.

Revised manuscript
2.5. Identification of extreme and normal levels of CH_4 and CO_2 concentrations and fluxes Pearson type III probability distribution curve (Hosking and Wallis, 1997), a widely used probability distribution function in hydrology and meteorological statistics (Sun and Qin, 1989), such as frequency analysis of extreme hydrological events, risk assessment of extreme climate, etc. (Raynal Villaseñor, 2021). Here, we employed Pearson type III probability distribution to determine the extreme and normal values of CH_4 and CO_2 concentrations and fluxes. The CH_4 and CO_2 concentrations and fluxes of all samples fitted the Pearson type III distribution well (Fig. S1; Kolmogorov-Smirnov test, $p > 0.05$).

Revised Supplementary Information
Text S3. Determination of extreme and normal values of greenhouse gases Meanwhile, the sample data points and the theoretical Pearson type III curve representing the population were plotted on the Hessian probability grid paper (Fig. S1), which is the most widely applied probability distribution function in hydrology and meteorological statistics (Sun and Qin, 1989). The differences between our dataset and the theoretical Pearson type III distribution were evaluated using the Kolmogorov-Smirnov test, with the sample data fitting the theoretical curve well

when $p > 0.05$.

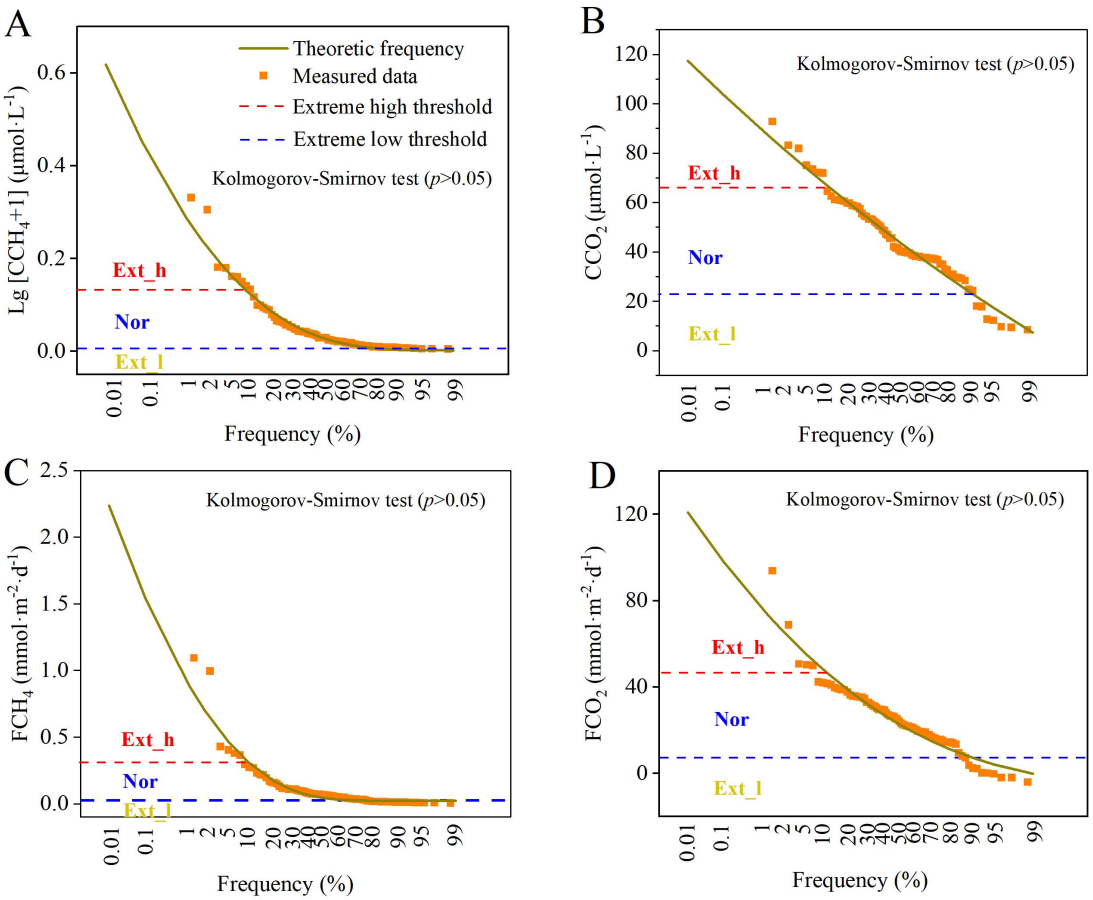

Fig. S2. Pearson type III curve analysis on CH_4 (A, C) and CO_2 (B, D) concentrations and fluxes. Ext_h, extremely high; Nor, normal; Ext_l, extremely low. CCH_4, and CCO_2 denote the concentration of CH_4, and CO_2 in the surface water column. FCH_4, and FCO_2 denote the flux of CH_4, and CO_2 across the water-air interface. The differences between measured data and the theoretical distribution of the Pearson type III frequency curve were evaluated using the Kolmogorov-Smirnov test, and $p > 0.05$ indicates that the dataset fits the theoretical curve well.

2) Aspect 1 (extreme value classification): Justify the 10% probability threshold for extreme values with ecological context (e.g., alignment with IPCC's "extreme event" definitions).

We thank you for pointing this out. According to the IPCC's definition, an extreme event (e.g., extreme weather or climate event) typically refers to an event with a low probability of occurrence that can induce sudden changes in ecosystems (IPCC, 2021). The IPCC generally uses a probability threshold to identify such extremes, with these events having a low probability, typically set at 10%. This means that events with a probability lower than 10% within a particular period and place are usually considered extreme (IPCC, 2021). Therefore, using a 10% probability threshold to define extremes is consistent with the ecological context and helps identify and study extreme events that have significant impacts on ecosystems. The rationale for using the 10% probability threshold in extreme identification has been added in section 2.5 of the revised manuscript. Specific revisions are below.

Revised manuscript
2.5. Identification of extreme and normal levels of CH_4 and CO_2 concentrations and fluxes Here, we employed Pearson type III probability distribution to determine the extreme and normal values of CH_4 and CO_2 concentrations and fluxes. The CH_4 and CO_2 concentrations and fluxes of all samples fitted the Pearson type III distribution well (Fig. S2; Kolmogorov-Smirnov test, $p > 0.05$). According to the IPCC's definition, an extreme event, e.g., an extreme weather or climate event, typically refers to an event with a low probability of occurrence that can induce sudden changes in ecosystems (IPCC, 2021). The IPCC generally uses a probability threshold to identify such extremes, with these events having a low probability, typically set at 10%. This means that events with a probability lower than 10% within a particular period and place are usually considered extreme (IPCC, 2021). Using a 10% probability threshold to define extremes is consistent with the ecological context and helps identify and study extreme events that have significant impacts on ecosystems. Therefore, in this study, we set the 10% probability ranges at the tails of both ends of the theoretical curve as the extreme values of CH_4 and CO_2 concentrations and fluxes (Ding and Jiang, 2009). Based on these threshold values, we divided the dataset into three groups, i.e. extremely high, normal, and extremely low.

3) Aspect 1 (microbial functional analysis): Include flow cytometry gating strategies and quality controls (e.g., negative controls for FCM, rarefaction curves for sequencing).

We thank you for pointing this out. The description regarding the gating strategies and negative controls for flow cytometry has been added in the second and third paragraphs of Supplementary Text S1 of the revised Supplementary Information. Additionally, the rarefaction curves for sequencing have been added in Fig. S1. Specific revisions are below.

Revised Supplementary Information
Text S1. Flow cytometry analysis The fluorescence signals detected by the flow cytometer result from the combination of the cell's non-specific fluorescence and the specific fluorescence of the stains. In order to determine the non-specific fluorescence, we set up the negative controls. Before analyzing the samples, we first analyzed the negative control (i.e., samples without fluorescent stains added) and set the voltage for each channel (Chen and Cao, 2014). The positive/negative boundary was determined based on the non-specific fluorescence signal values. Then, the samples with fluorescent stains added were analyzed, and cells with fluorescence signal values above the boundary were identified as positive cells. A total of 100,000 events were acquired for each sample. The cell concentration was computed by the sample flow rate and the the volume of sample plus additions (fixatives, beads, etc.) (Marie et al., 1999). Flow cytometer list mode files were collected, saved, and analyzed with CytoExpert software (Beckman Coulter® version 2.4, USA). The strategies for setting sorting gates can be summarized in three points: 1) exclude dead cells or fragments; 2) set the sorting gate at a relatively central

position between the two cell populations to avoid overlap; 3) eliminate adherent cells (Du and Feng, 2014). .

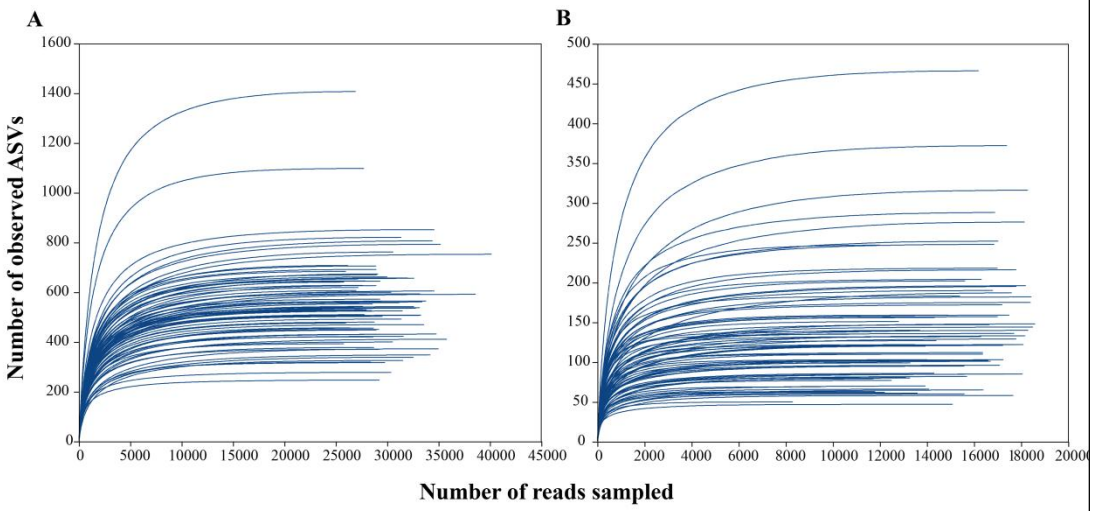

Fig. S1. Rarefaction curves for bacterioplankton (A) and phytoplankton (B) based on observed ASVs. Lines represent different samples

The results of rarefaction curves have been added in the second paragraph of section 2.3 of the revised manuscript. Specific revisions are below.

Revised manuscript
The PCR products of each sample were sequenced on the Illumina MiSeq platform at Majorbio Bio-Pharm Technology, Co., Ltd. (Shanghai, China). A total of 3,400,170 and 1,763,782 high-quality 16S rRNA and 23S rRNA sequences were generated for 78 samples. After subsampling each sample to an equal sequencing depth (43,591 reads per sample for bacterioplankton and 22,613 reads per sample for phytoplankton), we clustered the reads into ASV tables, obtaining 7,855 ASVs for bacterioplankton and 2,106 for phytoplankton. The number of ASVs per sample ranged from 39 to 147 for bacterioplankton and from 47 to 466 for phytoplankton.

The rarefaction curves displayed clear asymptotes (Fig. S1), indicating near-complete sampling of the community. DNA extraction, PCR amplification, and high-throughput sequencing were discussed in detail in the supplementary method S2.

4) Aspect 1 (microbial functional analysis): Briefly describe primer sets and PCR conditions for 16S/23S rRNA sequencing to ensure reproducibility.

We thank you for pointing this out. We have added the description of the primer sets and PCR conditions in the second paragraph of section 2.3 of the revised manuscript. Specific revisions are below.

Revised manuscript
Genomic DNA was extracted in duplicate from the filters using the FastDNA SPIN kit (Mo Bio laboratories®, USA), following the manufacturer's instructions. The duplicate DNA extracts were mixed for the following polymerase chain reaction (PCR) amplification. For phytoplankton, the 23S rRNA gene was amplified using the primer pair A23SrVF2 (5'-CARAAAGACCCTATGMAGCT-3') and A23SrVR2 (5'-TCAGCCTGTTATCCCTAG-3') (Yoon et al., 2016). For bacterioplankton, the V3-V4 regions of the bacterial 16S rRNA gene were amplified using the primer pair 338F (5'-ACTCCTACGGGAGGCAGCAG-3') and 806R (5'-GGACTACNNGGGTATCTAAT-3') (Ding et al., 2020). Amplicons were purified with an AxyPrep DNA Gel Extraction Kit (Axygen Biosciences, USA). The PCR amplification was performed in a 20 μL reaction system containing 1 μL

of DNA template, 0.8 μL of forward primer, 0.8 μL of reverse primer, 2 μL of 10×Buffer, 0.2 μL of BSA solution, and 2 μL of dNTPs (2.5 mM).

5) Aspect 2 (isotopic evidence): Discuss potential confounding effects of methanotrophy on $\delta^{13}C\text{-}CH_4$ values, particularly in hypoxic bottom waters. Clarify whether isotope measurements account for fractionation during gas exchange.

We thank you for pointing this out. In our study, we primarily focused on the variations in CH_4 and CO_2 concentrations and their isotopes in the water column. The processes of gas exchange at the water-air interface, such as dissolution and emission, were not considered and were assumed to cause negligible isotope fractionation. The potential effects of methane oxidation on CH_4 concentration and $\delta^{13}C$ have been discussed in the second paragraph of section 4.1 of the revised manuscript. We also have added the distribution of $\delta^{13}C\text{-}CH_4$ in extremely normal and high groups of CH_4 concentration in Fig. S8. Specific revisions are below.

Revised manuscript
This is probably because the decomposition of OC from phytoplankton preferentially releases ^{12}C and leaves the residual OC enriched in ^{13}C (van Breugel et al., 2005). Furthermore, microbial oxidation of CH_4 can influence both its concentration and carbon isotope. Methane-oxidizing bacteria (MOB) are capable of consuming CH_4 under either anoxic or oxic conditions (Reis et al., 2020), leading to ^{13}C enrichment of residual CH_4 (Whiticar and Faber, 1986). In freshwaters, the two main biological pathways of methanogenesis are acetate fermentation and CO_2/H_2 reduction (Preheim et al., 2016), both of which typically result in $\delta^{13}C\text{-}CH_4$ values

lower than -50‰ (Whiticar, 1999) (acetate fermentation:-60‰ to -50‰; CO_2/H_2 reduction: -60‰ to -110‰). In our study, most $\delta^{13}C$-CH_4 values observed in the surface water column were higher than -50‰ (Fig. S8), suggesting that CH_4 was indeed oxidized in the five investigated reservoirs. The optimal DO concentration for CH_4 oxidation by MOB is reported to range from 0.5 to 4 mg/L (Thottathil et al., 2019). Here, in all five reservoirs, DO concentrations in surface water were generally above 4 mg/L. It can be inferred that CH_4 oxidation in the surface water is limited, and a considerable proportion of CH_4 is more likely oxidized in the bottom water or bottom sediment layer. High productivity may also convert lakes or reservoirs from a CO_2 source to a sink (Balmer and Downing, 2011).

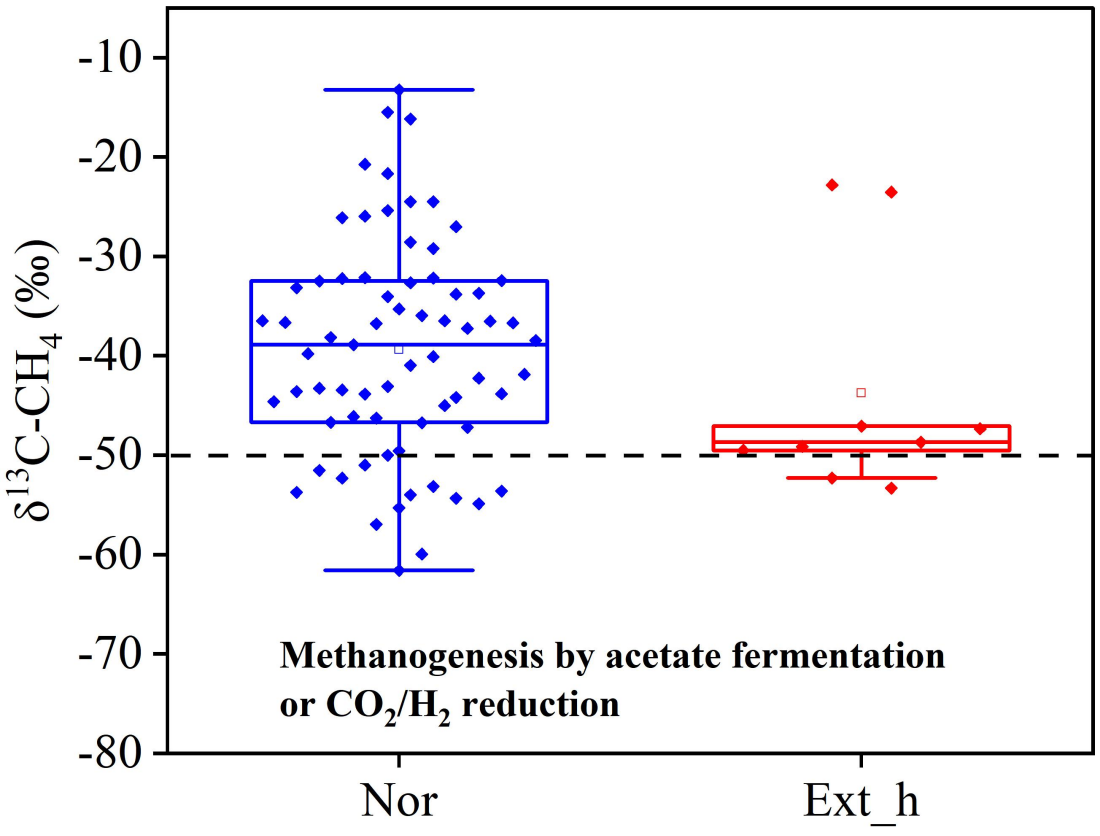

Fig. S8. Distribution of $\delta^{13}C$-CH_4 in extremely normal and high groups of CH_4

concentration. The $\delta^{13}C$-CH_4 of methanogenesis by acetate fermentation or carbonate reduction is below the black doted line at -50‰ (Whiticar., 1999).

6) Aspect 2 (isotopic evidence): Expand on the paradox of elevated $\delta^{13}C$-DOC in high-Chl-a conditions (Fig. 8B): Does this reflect preferential ^{12}C uptake by PP or HB-mediated degradation?

We thank you for pointing this out. Picophytoplankton can preferentially absorb the isotopically light CO_2 (^{12}C) as a C source through primary production, leading to ^{13}C depletion in the surface water organic carbon (Han et al., 2018), and $\delta^{13}C$-DOC therefore exhibits a negative correlation with picophytoplankton. However, in summer, picophytoplankton assimilate HCO_3^- as an alternative inorganic C source under CO_2 limitation during intense photosynthesis, which weakens the discrimination of ^{13}C and leads to ^{13}C enrichment of organic carbon (Fogel and Cifuentes, 1993). This can explain the significant positive linear correlation between δ13C-DOC and Chl-a in the extremely low group of CO_2 concentration (Fig. 8B). The explanation regarding the paradox of a significant positive correlation between $\delta^{13}C$-DOC and Chl-a has been added in the second paragraph of section 4.1 of the revised manuscript. Specific revisions are below.

Revised manuscript
Phytoplankton provides a large amount of autochthonous POC through photosynthesis, and picophytoplankton was therefore significantly correlated with POC ($p < 0.01$, Fig. 8A). Picophytoplankton can preferentially absorb the isotopically light CO_2 (^{12}C) as a C source through primary production, leading to ^{13}C depletion in the surface water organic carbon (Han et al., 2018), and $\delta^{13}C$-DOC

therefore exhibits a negative correlation with picophytoplankton. However, in summer, picophytoplankton may assimilate HCO_3^- as an inorganic C source under CO_2 limitation during intense photosynthesis, which weakens the discrimination of ^{13}C and enriches organic matter with ^{13}C (Fogel and Cifuentes, 1993). The above reasoning could explain the ^{13}C enrichment in the surface water DOC with the increase in Chl-a ($p < 0.01$, Fig. 8B).

7) Aspect 2 (PP-HB interaction mechanisms): Elaborate on how PP-HB cell aggregation (mentioned in Discussion) directly enhances CH_4 production. Does this relate to anoxic microenvironments or shared metabolic pathways (e.g., cross-feeding of vitamins)?

We thank you for pointing this out. The mechanism by which the aggregation of PP and HB cells enhances CH_4 production has been elaborated in the fourth paragraph of section 4.3 of the revised manuscript. Specific revisions are below.

Revised manuscript

Extremely high CH_4 concentrations and fluxes mainly occurred in July (Fig. 2A), and extremely high values of CH_4 concentration were positively influenced by PP abundance ($p < 0.001$; Fig. 7A). During summer algal bloom period, increased cell densities of PP and HB, induced by high nutrient inputs and elevated temperatures, would enhance the possibility of PP-HB interactions (Christie-Oleza et al., 2017). The intensified interactions, in turn, would promote the aggregation of their biomass. Increased aggregation of both PP and HB cells would increase carbon flux export to the bottom water column, providing sufficient substrates for

CH_4 production in the bottom layer (Gärdes et al., 2011) and creating a micro-anaerobic environment that favors CH_4 production (Tang et al., 2023; Zhou et al., 2023).

8) Aspect 2 (PP-HB interaction mechanisms): Contrast freshwater PP-HB dynamics with marine systems (Introduction/Discussion), highlighting unique aspects (e.g., terrigenous POC influence).

We thank you for pointing this out. We have added a comparison of the patterns of PP-HB interactions between freshwater and marine systems in the fourth paragraph of the *Introduction* of the revised manuscript. Specific revisions are below.

Revised manuscript
Marine and freshwater ecosystems exhibit distinct patterns of picophytoplankton-heterotrophic bacteria interactions: (i) picophytoplankton-regulated: In marine ecosystems, the interactions between picophytoplankton and heterotrophic bacteria appear to rely heavily on autochthonous POC produced by picophytoplankton through primary production (Morris et al., 2011); (ii) heterotrophic bacteria-regulated: In contrast, freshwater systems are closely linked to anthropogenic activities and act as collectors of large amounts of allochthonous POC from surrounding cities, towns, and farmlands (Wang et al., 2021). In these freshwater systems, picophytoplankton-derived autochthonous POC alone is insufficient to support heterotrophic bacterial growth, and the metabolic activity of heterotrophic bacteria primarily depends on allochthonous POC (Kritzberg et al., 2004). In addition, mineralization of

allochthonous POC by heterotrophic bacteria releases nutrients and inorganic carbon, which, in turn, stimulate picophytoplankton growth (Solomon et al., 2015).

9) Aspect 3 (SEM path coefficients): Report standardized effect sizes (β values) for SEM paths to quantify the relative importance of PP vs. HB in driving extremes (Fig. 7).

We thank you for pointing this out. In Fig. 7, we have added the standardized total effects of each variable on extreme and normal values of CH_4 and CO_2 to quantify the relative importance of PP and HB in driving extremes. The description of the standardized total effects has been added in the last paragraph of section 3.5 of the revised manuscript. Specific revisions are below.

Revised manuscript
In the extremely high group of CH_4 concentration, PP had the highest impact (0.90) on CH_4 concentration, followed by POCauto (0.42), POCallo (-0.31), and HB (-0.17) (Fig. 7F), based on the standardized total effects derived from the structural equation models depicted above. In the normal group, all variables had positive total effects on CH_4 concentration (Fig. 7G), with HB showing a slightly higher total effect than PP. In the extremely high group of CO_2 concentration, both PP and POCauto had positive total effects on CO_2 concentration (Fig. 7H). In the normal group of CO_2 concentration, only POCallo had a positive effect on CO_2 concentration (Fig. 7I). In the extremely low group of CO_2 concentration, POCauto had the highest impact on CO_2 concentration, followed by HB, PP, and POCallo (Fig. 7J).

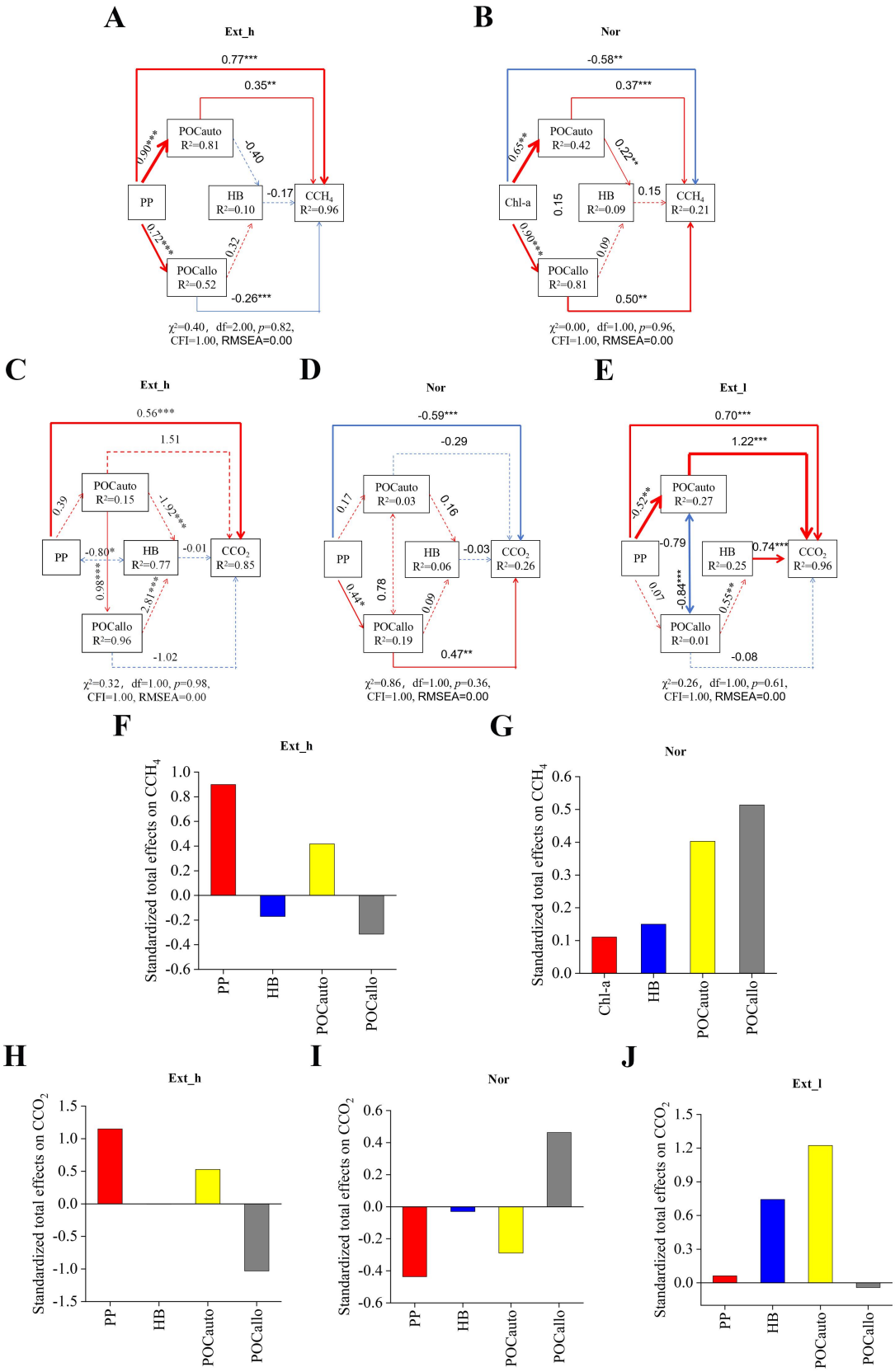

Fig. 7. Structural equation models (SEMs) describing selected variables' effects on the concentration of CH_4 (A, B) and CO_2 (C, D, E) in the extremely high (Ext_h), normal (Nor) and

extremely low (Ext_l) group, respectively. Numbers adjacent to arrows are standardized path coefficients and indicative of the effect size of the relationship. Solid arrows indicate significant paths (* $p < 0.05$, ** $p < 0.01$, *** $p < 0.001$), and dashed lines represent non-significant paths. The red and blue arrows indicate positive and negative path coefficients, respectively. The width of the arrows represents the strength of relationships. R^2 denotes the percentage of variance explained by the model. Standardized total (direct and indirect) effects of selected variables on the concentration of CH_4 (F, G) and CO_2 (H, I, J) in the extremely high (Ext_h), normal (Nor), and extremely low (Ext_l) group, respectively. PP, picophytoplankton; HB, heterotrophic bacterial; POCauto, autochthonous POC; POCallo, allochthonous POC; CCH_4 and CCO_2 were the concentrations of CH_4 and CO_2.

10) Aspect 3 (SEM path coefficients): Discuss why HB abundance showed no direct effect on CH_4 in SEM (Fig. 7A) despite high HB-PP correlations. Could functional genes (e.g., mcrA) resolve this discrepancy?

We thank you for pointing this out. In Fig. 7A, HB did not exhibit a significant direct effect on CH_4 concentration, despite strong HB-PP interactions. The possible reason is that, although HB are present, their potential for CH_4 production may vary depending on environmental conditions and microbial community activity. HB may influence CH_4 production at the functional level, which is not fully captured by HB abundance alone. Therefore, incorporating data on functional genes involved in methanogenesis, such as *mcrA*, could help clarify whether HB truly influence CH_4 production rather than relying solely on their abundance. The description has been added in the fourth paragraph of section 4.3 of the revised manuscript. Specific revisions are below.

Revised manuscript
Indeed, a significant positive correlation between network degree (i.e.,

interaction strength between HB and PP) and CH_4 concentrations and fluxes was found under eutrophic conditions (Fig. S14). Nevertheless, the SEM results indicated that HB did not exert a significant direct effect on extreme CH_4 concentrations under eutrophic conditions (Fig. 7A). A possible explanation is that HB may influence CH_4 production at the functional level, which is not fully reflected by HB abundance alone. Therefore, incorporating data on methanogenesis-related genes, such as methyl-coenzyme M reductase subunit A (*mcrA*), may help resolve this discrepancy. The strong positive correlation between PP-HB interactions and CH_4 concentrations and fluxes may support our third hypothesis; however, further validation through laboratory incubation experiments and functional gene analyses is still required.

11) Aspect 3 (Trophic State Gradients): Compare reservoir-specific results (e.g., Three Gorges vs. Xiaoba II) to assess how dam size/hydrology modulates POCauto contributions (Table S1).

We thank you for pointing this out. The comparison of dam-related and hydrological variables between TGR and XB II to assess how dam size or hydrology modulates autochthonous POC contributions has been added in the first paragraph of section 2.1 of the revised manuscript. Specific revisions are below.

Revised manuscript
XB II (with a total capacity of 11300 m^3) is a small reservoir only for drinking water supply located on a tertiary tributary named Ganxi Gulley of the Yangtze River. Compared to XB II, the TGR has a significantly larger dam size (total

storage capacity and water depth) and a longer hydraulic retention time (HRT) (Table S1). The greater depth in TGR promotes thermal stratification, which inhibits vertical mixing and facilitates nutrient accumulation in the hypolimnion. Meanwhile, sufficient light in the epilimnion supports phytoplankton growth and increases the production of autochthonous POC. The extended HRT in TGR reduces light attenuation and prolongs the retention of nutrients and phytoplankton in the water column, enhancing primary production and further promoting the accumulation of autochthonous POC. In contrast, the smaller dam size and shorter HRT in XB II weaken stratification, reduce nutrient retention, and limit phytoplankton growth, resulting in a lower contribution of autochthonous POC. The geographical and project information of these selected reservoirs is described in Table S1.

12) Aspect 3 (Trophic State Gradients): Address seasonal biases: Why were extreme CH_4 fluxes concentrated in July (Fig. 2A)? Link this to thermal stratification or monsoon-driven nutrient pulses.

We thank you for pointing this out. We have discussed why extremely high CH_4 fluxes mainly occurred in July (Fig. 2A) in relation to the nutrient pulse in the fourth paragraph of section 4.3 of the revised manuscript. Specific revisions are below.

Revised manuscript
In eutrophic reservoirs, the efficient production and rapid decomposition of easily degradable autochthonous POC by PP and HB, respectively, accelerate CH_4 production in the short term (West et al., 2012; Gärdes et al., 2011; Benassi et al.,

2021; Beaulieu et al., 2019). During the July monsoon peak, thermal stratification is often disrupted, and nutrients accumulated in the hypolimnion are rapidly transported to the epilimnion—a process known as a nutrient pulse. This nutrient pulse enhances PP-HB interactions (Jung et al., 2016), accelerates the turnover of autochthonous POC, and thereby results in the extremely high CH_4 concentrations and fluxes observed in July (Fig. 2A). Indeed, a significant positive correlation between network degree (i.e., interaction strength between HB and PP) and CH_4 concentrations and fluxes was found under eutrophic conditions (Fig. S14).

13) Aspect 4: Figure 2B: Simplify boxplot labels (e.g., use "Ext_L," "Nor," "Ext_H") and adjust axis scales for NO3−-N/SRP to reduce overlap.

We thank you for pointing this out. We have replaced "Extremely low", "Normal", and "Extremely high" with "Ext_l", "Nor", and"Ext_h", respectively, in Fig. 2B. We also adjusted the scales of the vertical axis for environmental parameters, such as NO_3^--N and SPR, in Fig. 2B to avoid overlap. The modified Fig. 2B is shown below.

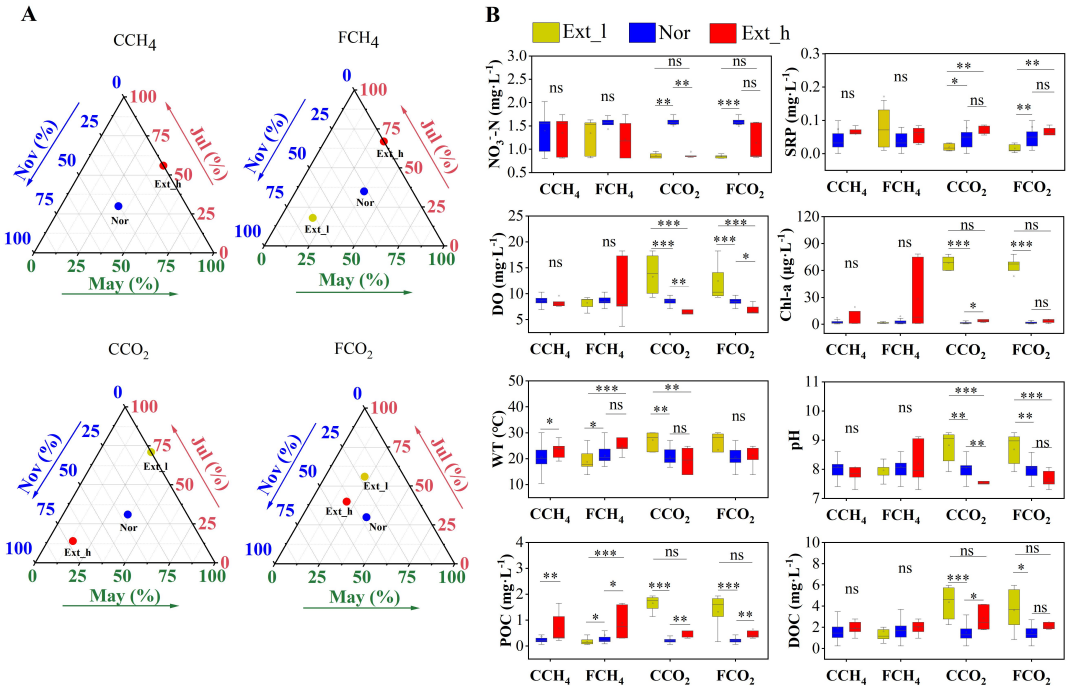

Fig. 2. Comparison of months and environmental parameters in extreme and normal groups. Panel A Ternary plots showing the percentage of months (May, July, and November) in which the extremely low (Ext_l), normal (Nor), and extremely high (Ext_h) values of CH_4 and CO_2 concentrations and fluxes occurred. The yellow, blue, and red dots represent the Ext_l, Nor, and Ext_h groups. Panel B Characteristics of NO_3^--N, SRP, DO, Chl-a, WT, pH, POC, and DOC in surface water. The yellow, blue, and red boxes represent environmental parameters in the extremely low (Ext_l), normal (Nor), and extremely high (Ext_h) groups of CH_4 and CO_2 concentrations and fluxes, respectively. Asterisks indicate significant difference: * $p < 0.05$, ** $p < 0.01$, *** $p < 0.001$.

14) Aspect 4: Figure 6: Add a legend for network edge colors (green = positive, violet = negative) and highlight keystone taxa (e.g., hub nodes) to emphasize PP-HB mutualism.

We thank you for pointing this out. We have identified the keystone taxa based on within-module connectivity (Zi) and among-module connectivity (Pi). The co-occurrence analysis, including the identification of keystone taxa, has been added

to Supplementary Text S6 of the revised Supplementary Information. Additionally, we have added the description of keystone taxa in the five networks in section 3.4 of the revised manuscript. We have also included a legend in Fig. 6 that illustrates edge colors and have labeled the keystone taxa using squares. Specific revisions are below.

Revised Supplementary Information
Text S6. Co-occurrence network The co-occurrence network (based on the ASV level) was constructed to disentangle potential interactions between bacterioplankton and phytoplankton. First, only amplicon sequence variants (ASVs) with a relative abundance > 0.1% of all samples were selected for correlation calculation (Xu et al., 2018). Pairwise correlation was then calculated based on the SparCC method, and only strong ($|r| > 0.6$) and significant ($p < 0.05$) correlations in the matrix were selected for further analysis (Hu et al., 2017). Networks were visualized in Gephi (v0.9.2). Network topological parameters of each sample, that is, subnetworks, were extracted using the subgraph function in the "igraph" package in R (Csardi and Nepusz, 2006). The nodes of each network were divided into four topological roles: (1) peripherals ($Zi \leq 2.5$, $Pi \leq 0.62$); (2) module hubs ($Zi > 2.5$, $Pi \leq 0.62$); (3) connectors ($Zi \leq 2.5$, $Pi > 0.62$); and (4) network hubs ($Zi > 2.5$, $Pi > 0.62$) (Olesen et al., 2007). Except for peripherals, the other three roles are considered keystone taxa (Banerjee et al., 2016). To identify keystone taxa, we calculated within-module connectivity (Zi) and among-module connectivity (Pi) using the "igraph" package in R (Fig. S4).

Revised manuscript

3.4. Interactions between phytoplankton and bacterioplankton communities

The co-occurrence patterns of phytoplankton and bacterioplankton in the extreme and normal groups of CH_4 and CO_2 concentrations were determined using network analysis (Fig. 6; Table 3). Overall, the number of nodes ranged from 101 to 184 in all five interaction networks. Most networks consisted of more than 50% positive edges, except in networks for the normal group of CO_2 concentration. In addition, topological properties of the co-occurrence network in normal groups of CH_4 and CO_2, such as modularity, were higher than those in the extreme groups. In contrast, the average degree showed an exactly opposite trend. The number of phytoplankton-bacterioplankton links decreased from 977 in the extremely high group to 104 in the normal group of CH_4 concentration (Fig. 6A and B). Similarly, the number of phytoplankton-bacterioplankton links in the normal group was also significantly lower than both in the extremely high and extremely low groups of CO_2 concentration (Fig. 6C-E). Compared with communities in normal groups, communities in the extreme groups exhibited a higher interaction strength (that is, links) between phytoplankton and bacterioplankton. A total of 53 keystone taxa were identified from five networks (Fig. 6; Fig. S4), and the taxonomic information of these keystone taxa was listed in Table S4. These keystone taxa belong to bacterial clades including Proteobacteria, Actinobacteriota, and Bacteroidota, as well as phytoplankton clades such as Cyanobacteria and Bacillariophyta.

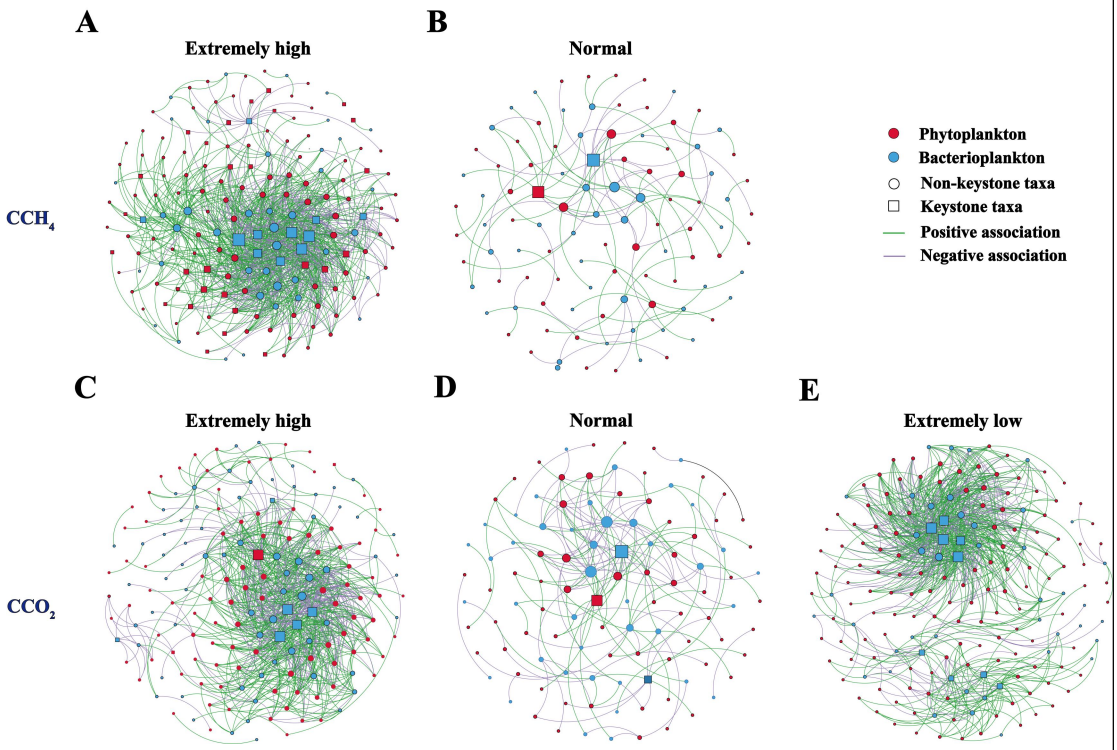

Fig. 6. Co-occurrence networks of phytoplankton and bacterioplankton communities based on correlation analysis. Panels A and B Co-occurrence patterns of phytoplankton-bacterioplankton interaction network in extremely high and normal groups of CH_4 concentration (CCH_4). Panels C, D, and E Co-occurrence patterns of phytoplankton-bacterioplankton interaction network in extremely high, normal, and extremely low groups of CO_2 concentration (CCO_2). Each line represents a significant correlation between the two taxa, with the green lines representing positive correlations and the violet lines representing negative correlations. The number of links represents the strength of interactions between phytoplankton and bacterioplankton. The red and blue nodes in each network represent phytoplankton and bacterioplankton, respectively. The size of each node is proportional to the number of connections (that is, degree). Circles and squares represent non-keystone taxa and keystone taxa, respectively. The taxonomic information of these keystone taxa was listed in Table S4.

15) Aspect 4: Supplement: Include a conceptual diagram summarizing the POCauto-PP-HB-CH_4/CO_2 pathway to guide readers.

We thank you for pointing this out. The conceptual summary of carbon (CH_4 and

CO_2) emission patterns under the influence of PP-HB interactions on POC from different sources is shown below.

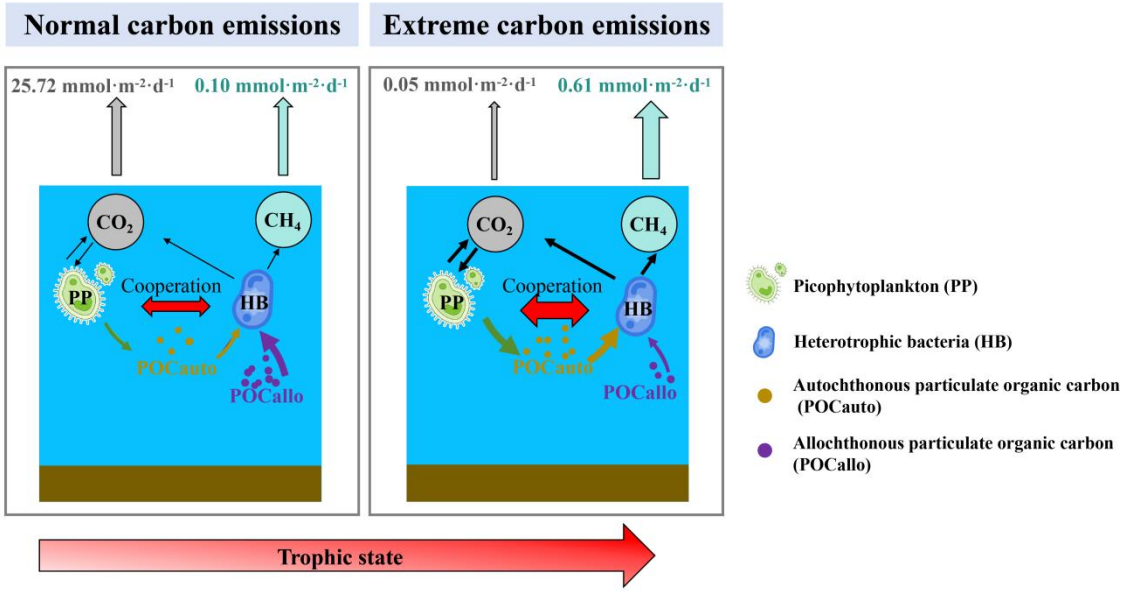

Minor comments included 3 points.

1) Define abbreviations at first use (e.g., TLI in Table 2, SEM in Fig. 7).

We thank you for pointing this out. The full name of TLI (trophic level index) has been added to the caption of Table 2. In addition, the full name of SEM (structural equation model) has been included in the caption of Fig. 7.

2) Cite recent studies on reservoir eutrophication and CH_4 emissions.

We thank you for pointing this out. We have cited recent studies on reservoir eutrophication and CH_4 emissions in the fourth paragraph of section 4.3 of the revised manuscript. Specific revisions are below.

Revised manuscript
These findings help explain why strong positive interaction strength (number of links) between phytoplankton and bacterioplankton was found in extreme carbon groups (eutrophic state) compared with normal groups (mesotrophic state) (Fig. 6).

In eutrophic reservoirs, the efficient production and rapid decomposition of easily degradable autochthonous POC by PP and HB, respectively, accelerate CH_4 production in the short term (West et al., 2012; Gärdes et al., 2011; Benassi et al., 2021; Beaulieu et al., 2019).

3) Check consistency in decimal places (e.g., 0.07 vs. 0.070 mg·L−1 in Fig. S4).

We thank you for pointing this out. I have corrected the decimal places in the first paragraph of section 3.2 of the revised manuscript to ensure consistency throughout the paper. Specific revisions are below.

Revised manuscript
The POCauto and POCallo concentrations in whole dataset respectively ranged from 0.00 to 0.86 $mg \cdot L^{-1}$ and 0.05 to 1.77 $mg \cdot L^{-1}$, and were positively correlated with TLI.